球磨方式对锂离子正极材料 $LiFePO_4$ 性能的影响

唐致远*,[1] 高 飞[1] 薛建军[2]
([1]天津大学化工学院,天津 300072)
([2]广州鹏辉电池有限公司,广州 511483)

摘要: 采用高温固相合成法制备橄榄石型的 $LiFePO_4$ 正极材料,在合成过程中分别采用湿法球磨和干法球磨两种球磨方式。用 X-射线衍射,扫描电镜,激光粒度测试等对合成材料进行表征,并对以 $LiFePO_4$ 为正极的电池进行电化学性能测试。结果表明,相对于干法球磨,湿法球磨制备的 $LiFePO_4$ 样品具有更好的电化学性能,0.2C 放电的首次放电比容量为 134.9 $mAh\cdot g^{-1}$,并有优良的大电流放电性能及循环性能。这主要是因为采用湿法球磨制备的 $LiFePO_4$ 材料物相较纯、粒径均匀,与导电添加剂的接触更加紧密,从而提高了 $LiFePO_4$ 材料电化学性能。

关键词: 磷酸铁锂; 球磨; 粒径; 正极材料; 锂离子电池
中图分类号: O614.111; TM912.9 **文献标识码**: A **文章编号**: 1001-4861(2007)08-1415-06

Effects of Ball-milling on the Preparation of $LiFePO_4$ Cathode Material for Lithium-ion Batteries

TANG Zhi-Yuan*,[1] GAO Fei[1] XUE Jian-Jun[2]
([1]*School of Chemical Engineering and Technology, Tianjin University, Tianjin* 300072)
([2]*Great Power Battery Co., Ltd, Guangzhou* 511483)

Abstract: Olivine $LiFePO_4$/C composite powders were synthesized by solid-state reaction with wet ball-milling procedure. The powder properties and the electrochemical characteristics of the prepared samples were investigated in comparison with those samples obtained by dry ball-milling. The crystal structure and the electrochemical performance were characterized by XRD, SEM, laser particle-size distribution measurement and electrochemical performance testing. The olivine $LiFePO_4$ obtained from wet ball-milling shows a maximum discharge capacity of 134.9 $mAh\cdot g^{-1}$ at the C/5 rate. The composite also displays a better rate capability, a higher charge-discharge capacity and a more stable cycle-life than those samples from dry ball-milling. The improved electrode performance of samples by wet ball-milling originates mainly from very fine particles of sub-micron size and a homogeneous surface morphology. These powder characteristics increase the surface area of $LiFePO_4$ particles and maximize the contact area with the conductor additives, resulting in enhanced electrochemical performance.

Key words: lithium iron(Ⅱ) phosphate; ball-milling; particle size; cathode material; lithium-ion batteries

Lithium ion batteries are key components of mobile telephones and portable computers. Among the known Li-intercalation materials for lithium ion battery cathodes, $LiCoO_2$, $LiNiO_2$, and $LiMn_2O_4$ have been studied extensively[1~4]. $LiCoO_2$ is now used in commercial lithium-ion batteries despite its high cost and

收稿日期:2007-04-16。收修改稿日期:2007-06-04。
国家自然科学基金资助项目(No.2027304)。
*通讯联系人。E-mail:zytang@tju.edu.cn
第一作者:唐致远,男,61 岁,教授,博士生导师;研究方向:化学电源。

toxicity. It is difficult to prepare $LiNiO_2$ material. $LiMn_2O_4$ has been a promising candidate because of its low toxicity and low cost compared to $LiCoO_2$ and $LiNiO_2$, but its structure tends to change because of a cooperative Jahn-Teller deformation, which reduces its capacity irreversibly.

Recently, olivine-structured $LiFePO_4$ is gaining interest as a candidate material for rechargeable lithium-ion batteries from both an economic and environmental point of view. It has an ordered olivine-type structure (S.G.: *Pnmb*), in which Li, Fe and P atoms occupy octahedral 4a, octahedral 4c and tetrahedral 4c sites, respectively. The FeO_6 octahedra are separated by PO_4 polyanions in $LeFePO_4$ triphylite, which significantly reduces the kinetic performance. Therefore it has a highly stable three dimensional framework due to strong P-O covalent bonds in PO_4^{3-} polyanion, which prohibits the liberation of oxygen [5]. These characteristics provide an excellent safety and a stable operation of battery even under unusual conditions[6~9].

$LiFePO_4$ is generally synthesized by solid-state reaction at a higher temperature (for example: 700 ℃) to enhance the diffusion process and obtain a well-ordered structure. Owing to this high temperature, there are some disadvantages such as broader particle size distribution, longer reaction time and undesirable impurities. To overcome these disadvantages, numerous attempts[10~14] were made by milling start materials and finished products such as blending start materials uniformly and decreasing the size of the particles of finished products. Mechanical milling, which can be viewed as the action of transforming mechanical energy into chemical energy, stands as a simple and environmentally friendly alternative to high temperature synthesis or solution chemistry. It enables the room temperature elaboration of metastable phases (either crystallized or amorphous), which are unreachable via classical routes, and provides a convenient means to change the morphology of powders. However, sometimes the mixtures of start materials are not absolutely uniform by the dry milling, thus resulting in undesirable impurities. Moreover, bulky aggregates or a partly amorphous powder would be formed in the subsequent dry milling process.

The wet milling (by adding a liquid as moderator in the vial together with powders and milling balls) decreases the intensity of the shocks, thus reducing the degradation of fragile materials. In addition, the presence of a liquid prevents from the sticking of the particles and decreases the surface tension. The resulting powder is completely different from that prepared by dry milling in terms of the grain agglomerations.

1 Experimental

The carbon-containing $LiFePO_4$ compounds were prepared by solid-state reaction. The precursors of Li_2CO_3 (99.9% Aldrich), $FeC_2O_4 \cdot 2H_2O$ (98% Aldrich), $NH_4H_2PO_4$ (99.5% Aldrich) and acetylene black (Mitsubishi Chemicals), were mixed in a stoichiometric ratio (molar rate of Li^+:Fe^{2+}:(H_2PO_4):C=1.02:1:1:0.5). First, the precursors were ground for 12 h by wet ball-milling in ethanol solution to ensure intimate and homogeneous mixing. The wet ball milled fine powders of the precursor mixtures were dried at 80 ℃. Then the dried powders were subjected to calcination temperature of 300 ℃ for 6 h at first and then to 700 ℃ for 16 h (heating ramp: 5 ℃·min^{-1}) in a rotary furnace with N_2 + 5%H_2 (*V*/*V*) atmosphere. The rotation rate of the rotary furnace was 1 r·min^{-1}. Finally, the samples were reground for 8 h by wet ball-milling in ethanol solution after they were cooled to room temperature in the rotary furnace and the final product of carbon-containing $LiFePO_4$ was obtained. The sample synthesized by wet ball-milling was denoted as LFP1.

For comparison, sample was also synthesized by dry ball-milling under the same synthesis parameters. The sample synthesized by dry ball-milling was denoted as LFP2.

The structure and phases of the $LiFePO_4$ thin-film samples were characterized by X-ray diffraction (RU-200B/RINT, Rigaku, Rotaflex using monochromatic Cu $K\alpha$ radiation λ=0.154 18 nm, 35 kV, 25 mA, Detector: Scintllation Counter, step scanning: 0.02°). The morphology of the thin-film samples was recorded by

using a scanning electron microscopy (JSM-6330F, high vacuum, 10 keV). The particle size distribution was investigated by particle size analysis (PSA). The specific surface area of the powder particles was estimated by the BET method (Gemini V-2380).

Thin film electrodes were manufactured for electrochemical testing of the samples by casting on an aluminum current collector a *N*-methylpyrrolidone (NMP) slurry of the $LiFePO_4$ active material (82wt.%) mixed with a carbon black (Super P-Timcal) conductive additive (10wt.%) and a polyvinylidene fluoride (Kyner2801-Eif Atochem) binder (8wt.%). These film-type $LiFePO_4$ electrodes were assembled in a nitrogen filled glove box using MCMB anode as a counter electrode. The electrolyte was 1 $mol \cdot L^{-1}$ $LiPF_6$ in a mixture of ethylene carbonate (EC) and diethyl carbonate (DMC) (1∶1, *V*/*V*). The cells were charged and discharged over a voltage range of 2.0~3.8 V.

Cyclic voltammetry (CV) measurements were performed using a Voltalab systems with VM4 (Model PGZ301) between 2.0 V and 4.2 V at a scan rate of 0.1 $mV \cdot s^{-1}$. These tests were performed using a three-electrode cell. The thin film electrodes of $LiFePO_4$ were used as working electrodes. The counter and reference electrodes were lithium foil.

2 Results and discussion

2.1 XRD analysis

The XRD pattern (Fig.1a) of the sample LFP1 shows an absence of parasitic peaks, and all the diffraction peaks can be indexed on the orthorhombic structure with the space group *Pnmb*, in agreement with a well crystalline single phase $LiFePO_4$ according to the PDF2 (83-2092). The lattice parameters of well-crystallized $LiFePO_4$ are a=0.601 9 nm, b=1.034 7 nm and c=0.470 4 nm, according to the PDF2. And there is no evidence for carbon diffraction peaks, indicating that the residual pyrolytic carbon in product is amorphous or the level of the carbon is below the detection limit. For comparison, the XRD pattern (Fig.1b) of the sample LFP2 shows parasitic peaks (marked by arrow in Fig.1b) due to impurities which are considered to be iron (Ⅱ, Ⅲ) pyrophosphates or phosphates (perhaps $Li_3Fe_2(PO_4)_3$ or $LiFe(P_2O_7)$). The nonuniformity of the mixture with dry ball-milling and high temperature results in impurities. So the wet ball-milling is preferred. Though the wet milling decreases the intensity of the shocks, the nicer fluidity of the mixture ensures the uniformity of the mixtures.

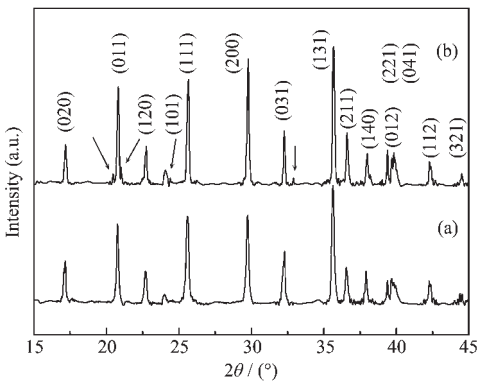

Fig.1　XRD patterns of the $LiFePO_4$ from (a) wet ball-milling, (b) dry ball-milling

It should be noted that the peak width of the LFP1 in the XRD patterns is greater than that of the LFP2. For example, the (131) peak width of LFP1 is obviously wider than that of LFP2, which means that wet ball-milling causes a decrease in the crystalline grain size of the samples. The grain size (D) based on the (131) diffraction peak was estimated using the Scherrer formula. The D_{131} values estimated from the (131) peak width are 73 nm for LFP1 and 85 nm for LFP2. The grain size decreases with the wet ball-milling.

2.2 Morphology

Fig.2 shows the scanning electron micrographs of LFP1, LFP2 compounds from (a) wet ball-milling and (b) dry ball-milling. The particles of the powders display nonuniformity. The particle size of the LFP1 is about 0.5~2 μm (Fig.2a), whereas LFP2 particles congregate together and grow up to larger particles ranged from 0.5 to 4 μm (Fig.2b). Obviously, the particle size of the synthesized powders is larger than its grain size, implying that the particles are formed from the agglomeration of several grains. Because repeated ball-milling, upon increasing the mechanical energy, will result in the cracks of the particles and the creation of new fresh surfaces. The successive fracture of

the particles will lead to a size decrease, which is therefore not unlimited since the increasing particles surface energy can outweigh the mechanical constraint energy, in which case the particles are going to form aggregates[15].

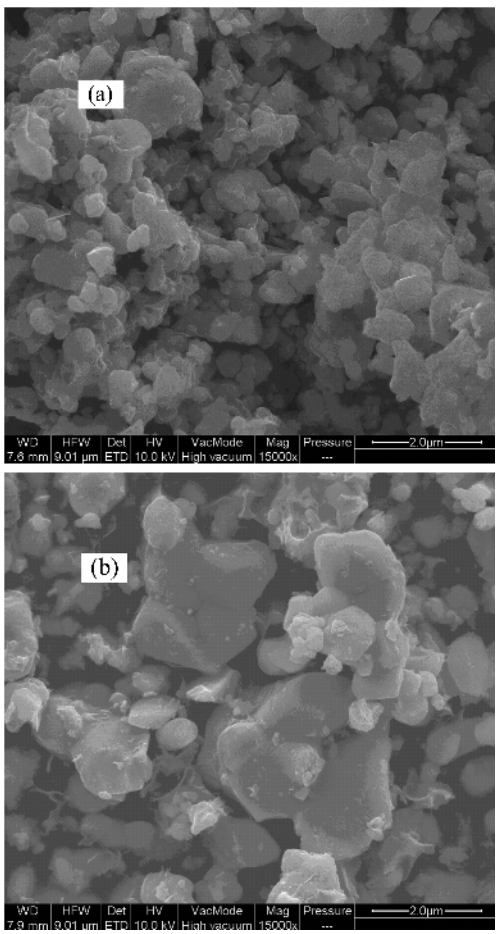

Fig.2 SEM photos of the $LiFePO_4$ from (a) wet ball-milling, (b) dry ball-milling

Fig.3 shows the particle size distribution measured by laser diffraction and scattering method. The LFP1 powder consists of 0.5~2 μm particles, and the average particle size, represented by the value at 50% cumulative distribution (d_{50}), is 1.14 μm. In contrast, the population of larger particles (>3 μm) for the dry ball-milling treatment drastically increased, resulting in larger d_{50} value (2.39 μm), which is consistent with the presence of agglomerates (>3 μm) in SEM observations. The specific surface area of the powder particles was measured by the low temperature Nitrogen adsorption and desorption method. The BET specific surface area of the LFP1 and LFP2 are 16, 11 $cm^2 \cdot g^{-1}$ respectively. Obviously, the dry ball-milling and the presence of agglomerated active particles decrease the specific surface area.

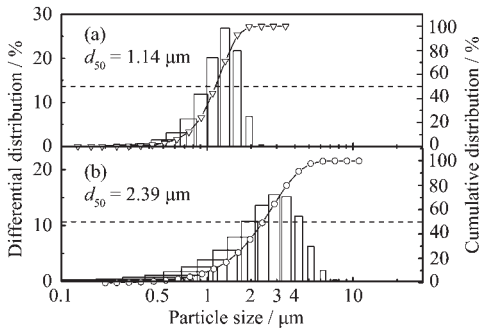

Average particle size is represented by the value at 50% cumulative population (d_{50})

Fig.3 Particle size distribution measured by laser diffraction and scattering method for LFP1, LFP2 compounds from (a) wet ball-milling, (b) dry ball-milling

2.3 Electrochemical properties

The CV profiles of LFP1 and LFP2 in the first cycle are shown in Fig.4. The voltage range was from 2.0 to 4.2 V, and the scan rate was 0.1 $mV \cdot s^{-1}$ at room temperature. The CV curves show one pair of peaks at about 3.6 V and 3.2 V, consisting of an oxidation peak and a reduction peak, respectively, and corresponding to the two-phase charge-discharge reaction of the Fe^{2+}/Fe^{3+} redox couple. Furthermore, the CV curves of LFP2 sample (Fig.4b) show phase inhomogeneity at 2.8~2.9 voltage range and this result may be caused by the redox potential of the $Li_3Fe_2(PO_4)_3$[16].

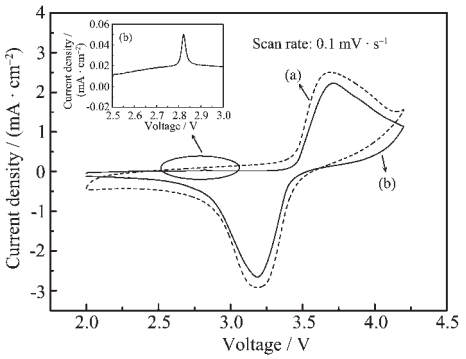

Fig.4 Cyclic voltammograms of the $LiFePO_4$ from (a) wet ball-milling, (b) dry ball-milling

The variation of the first discharge capacity of LFP1 and LFP2 with discharge rate is presented in Fig.5. With the increasing in current density, the dis-

charge voltage and the plateau voltage are rapidly reduced in both samples. The discharge capacity of LFP1 and LFP2 respectively decreases from 134.9, 128.6 $mAh \cdot g^{-1}$ at the C/5 rate to 129.4, 123.2 $mAh \cdot g^{-1}$ at the 1C rate.

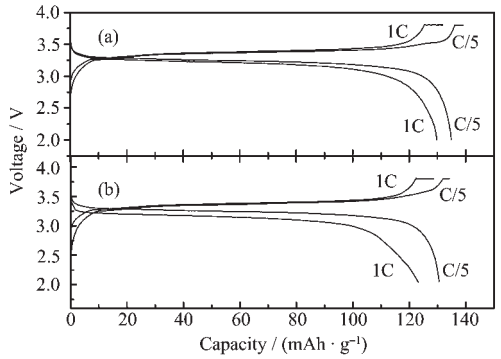

Fig.5　Charge-discharge curves at various rates for $LiFePO_4$ from (a) wet ball-milling, (b) dry ball-milling

The cycle performance of $LiFePO_4$ compounds by various milling is given in Fig.6. The experiments were performed in the range 2.0~3.8 V at 1C. For the batteries with the LFP1 as cathode materials, the capacity remains 99.4% after 100 cycles, showing better cycling stability. For the LFP2, the discharge capacities are decreased down to about the 10th cycle, and then become stabilized. After 100 cycles, the capacity remains 96.1%. According to Andersson's theory[17], during the charge-discharge process, lithium-ions and electrons have to move out through the newly formed $FePO_4$ phase. When lithium re-insertion takes place from the outside of the particle inwards, a new annular $LiFePO_4$ / $FePO_4$ interface moves quickly through the particle, and approaches the unconverted $LiFePO_4$ region at the center of the particle. This region does not recombine with the inaction $LiFePO_4$; instead, an annular region of $FePO_4$ is left trapped around the $LiFePO_4$ core, which results in a capacity loss. The essential source of capacity loss of LFP2 is, thus, the unconverted $LiFePO_4$ at the center of the larger particles, since it is not possible to extract all lithium-ions and electrons efficiently. Whereas, the smaller particle size of LFP1 can provide more surface area for lithium-ion diffusion and avoid the formation of the inaction $LiFePO_4$. Thus the LFP1 exhibits relatively superior cycle stability.

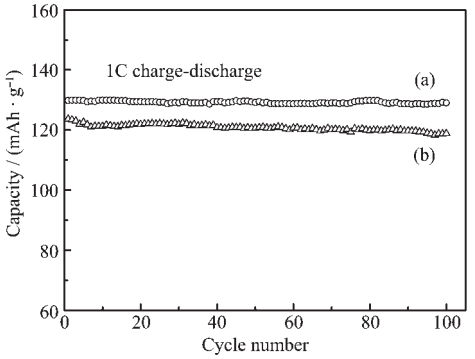

Cycled between 2.0 and 3.8 V, 1C

Fig.6　Cycle-life of $LiFePO_4$/C composite from (a) wet ball-milling, (b) dry ball-milling

3　Conclusions

The milling is an important procedure in the synthesis process of $LiFePO_4$. Owing to the presence of a fluid, the wet ball-milling offers very fine particles in sub-micron size range and a homogeneous surface morphology of the $LiFePO_4$ composites. The smaller particle size leads to a better electrode performance, resulting in an increase of the reversible specific capacity and better capacity retention with cycling. The discharge capacity of $LiFePO_4$ is 134.9 $mAh \cdot g^{-1}$ at the C/5 rate and 129.4 $mAh \cdot g^{-1}$ at the 1C rate. After 100 cycles at a current 1C, the capacity remains 99.4%. When dry ball-milling replaces wet ball-milling, the discharge capacity of $LiFePO_4$ is 128.6 $mAh \cdot g^{-1}$ at the C/5 rate and 123.2 $mAh \cdot g^{-1}$ at the 1C rate. After 100 cycles at a current 1C, the capacity only remains 96.1%. Consequently, the wet ball-milling technique offers a promising synthetic process to control the particle size of olivine-type $LiFePO_4$/C composite cathode materials for rechargeable lithium batteries.

References:

[1] Wu H M, Tu J P, Yuan Y F, et al. *Mater. Chem. Phys.*, **2005**, **93**:461~465

[2] Toshihide Tsuji, Hideaki Umakoshi, Yasuhisa Yamamura, et al. *J. Phys. Chem. Solids*, **2005**,**66**:283~287

[3] LI Xiao-Xia, CHENG Fang-Yi, GUO Bing. *J. Phys. Chem. B*, **2005**,**109**:14017~14024

[4] Youngjoon S, Manthiram A. *J. Power Sources*, **2004**,**126**:169~174

[5] Padhi A K, Nanjundaswamy K S, Goodenough J B, et al. *J. Electrochem. Soc.*, **1997**,**144**:1188~1194

[6] Kazuo Onda, Takamasa Ohshima, Masato Nakayama, et al. *J. Power Sources*, **2006**,**158**:535~542

[7] Nukuda T, Inamasu T, Fujii A, et al. *J. Power Sources*, **2005**, **146**:611~616

[8] Aniruddha Deb, Uwe Bergmann, Cramer S P, et al. *Electrochimica Acta*, **2005**,**50**:5200~5207

[9] CHEN Jia-Jun, Stanley Whittingham M. *Electrochem. Commun.*, **2006**,**8**:855~858

[10]Jayaprakash N, Kalaiselvi N. *Electrochem. Commun.*, **2007**, **9**:620~628

[11]Raphael Janot, Daniel Guerard. *Progress in Materials Science*, **2005**,**50**:1~92

[12]Rabanal M E, Gutierrez M C, Garcia-Alvarado F, et al. *J. Power Sources*, **2006**,**160**:523~528

[13]Jean-Marie Tarascon, Mathieu Morcrette, LucAymard C R. *Chimie*, **2005**,**8**:17~26

[14]Belharouak I, Johnson C, Amine K. *J. Power Sources*, **2003**, 119~121:252~257

[15]Hsu Kuei-Feng, Tsay Sun-Yuan, Hwang Bing-Joe. *J. Power Sources*, **2005**,**146**:529~533

[16]Park K S, Son J T, Chung H T. *Electrochem. Commun.*, **2003**, **5**:839~843

[17]Andersson A S, Thomas J O. *J. Power Sources*, **2001**,**97~98**: 498~502